Virtual Ligand Screening of the p300/CBP Histone Acetyltransferase: Identification of a Selective Small Molecule Inhibitor

Erin M. Bowers,[1] Gai Yan,[2] Chandrani Mukherjee,[1] Andrew Orry,[3] Ling Wang,[1] Marc A. Holbert,[1] Nicholas T. Crump,[4] Catherine A. Hazzalin,[4] Glen Liszczak,[5] Hua Yuan,[5] Cecilia Larocca,[2] S. Adrian Saldanha,[6] Ruben Abagyan,[7] Yan Sun,[1] David J. Meyers,[1] Ronen Marmorstein,[5,8] Louis C. Mahadevan,[4] Rhoda M. Alani,[2,9,*] and Philip A. Cole[1,2,*]
[1]Department of Pharmacology and Molecular Sciences
[2]Department of Oncology
Johns Hopkins University School of Medicine, Baltimore, MD 21205, USA
[3]Molsoft LLC, La Jolla, CA 92037, USA
[4]Nuclear Signalling Laboratory, Department of Biochemistry, Oxford University, Oxford OX1 3QU, UK
[5]Program in Gene Expression and Regulation, The Wistar Institute, Philadelphia, PA 19104, USA
[6]The Scripps Research Institute, Jupiter, FL 33458, USA
[7]Skaggs School of Pharmacy and Pharmaceutical Sciences, University of California, San Diego, La Jolla, CA, 92093, USA
[8]Department of Chemistry, University of Pennsylvania, Philadelphia, PA 19104, USA
[9]Present address: Department of Dermatology, Boston University School of Medicine, Boston, MA 02118-2515, USA
*Correspondence: pcole@jhmi.edu (P.A.C.), ralani@jhmi.edu (R.M.A.)
DOI 10.1016/j.chembiol.2010.03.006

SUMMARY

The histone acetyltransferase (HAT) p300/CBP is a transcriptional coactivator implicated in many gene regulatory pathways and protein acetylation events. Although p300 inhibitors have been reported, a potent, selective, and readily available active-site-directed small molecule inhibitor is not yet known. Here we use a structure-based, in silico screening approach to identify a commercially available pyrazolone-containing small molecule p300 HAT inhibitor, C646. C646 is a competitive p300 inhibitor with a K_i of 400 nM and is selective versus other acetyltransferases. Studies on site-directed p300 HAT mutants and synthetic modifications of C646 confirm the importance of predicted interactions in conferring potency. Inhibition of histone acetylation and cell growth by C646 in cells validate its utility as a pharmacologic probe and suggest that p300/CBP HAT is a worthy anticancer target.

INTRODUCTION

The reversible acetylation of histones and other proteins rivals protein phosphorylation as a major mechanism for cellular regulation (Walsh, 2006; Choudhary et al., 2009; Macek et al., 2009). Acetylation on protein lysine residues is catalyzed by histone acetyltransferases (HATs) and acetyl-Lys cleavage is performed by histone deacetylases (HDACs) (Hodawadekar and Marmorstein, 2007; Haberland et al., 2009; Cole, 2008). These enzymes and the associated acetylation events have been implicated in a wide variety of physiological and disease processes. In this study, we focus on the paralog HATs p300 and CBP (referred to as p300/CBP), which were originally discovered as E1A onco-

protein binding partners and cyclic AMP effectors, respectively (Goodman and Smolik, 2000). p300/CBP often serves as a transcriptional coactivator and has been suggested to bind to a range of important transcription factors (Goodman and Smolik, 2000). In 1996, p300/CBP was reported to possess intrinsic HAT activity (Ogryzko et al., 1996; Bannister and Kouzarides, 1996). Over the ensuing years, p300/CBP has been shown to be a rather promiscuous acetyltransferase, with more than 75 protein substrates described including p53, MyoD, and NFκB (Gu and Roeder, 1997; Yang et al., 2008; Wang et al., 2008). Dissecting the importance of the enzymatic activity of p300/CBP as opposed to its protein recruitment functions in clarifying p300/CBP's biological roles would benefit from selective cell-permeable HAT inhibitors. Recent studies suggest that the biologic functions of p300/CBP HAT activity may be associated with tumorigenesis, and it is therefore plausible that p300/CBP HAT inhibitors may serve as potential anticancer agents (Dekker and Haisma, 2009; Iyer et al., 2007).

Although studies on histone deacetylases have led to the discovery of highly potent compounds with clinical impact in cancer, the identification of histone acetyltransferase inhibitors has proved more challenging (Cole, 2008). Several reports of p300/CBP HAT inhibitors identified through screens or based on bisubstrate analogs have been published (Lau et al., 2000b; Thompson et al., 2001; Zheng et al., 2005; Guidez et al., 2005; Liu et al., 2008a; Stimson et al., 2005; Balasubramanyam et al., 2003; Balasubramanyam et al., 2004; Mantelingu et al., 2007; Arif et al., 2009; Ravindra et al., 2009). The most potent and selective compound, Lys-CoA (K_i = 20 nM), has been converted to a cell-permeable form with Tat peptide attachment (Lys-CoA-Tat) and has been used in a variety of studies, but its complexity is somewhat limiting for pharmacologic applications (Lau et al., 2000a; Thompson et al., 2001; Zheng et al., 2005; Guidez et al., 2005; Liu et al., 2008b). High-throughput screening experiments have led to several small molecule synthetic agents and natural product derivatives of moderate potency as p300 HAT inhibitors

(micromolar K_i values), but their selectivity and mechanism of inhibition remain to be fully characterized (Stimson et al., 2005; Balasubramanyam et al., 2003; Balasubramanyam et al., 2004; Mantelingu et al., 2007; Arif et al., 2009; Ravindra et al., 2009).

A recent high-resolution X-ray structure of the p300 HAT in complex with the bisubstrate analog Lys-CoA has revealed key aspects of substrate recognition and catalytic mechanism (Liu et al., 2008a). A narrow tunnel in p300 accommodates Lys-CoA, and the inhibitor makes a range of hydrogen bonding and Van der Waals interactions with the HAT active site (Liu et al., 2008a). Based on this structure and steady-state kinetic studies, a Theorell-Chance catalytic mechanism has been proposed (Liu et al., 2008a). This "hit and run" kinetic mechanism involves initial, stable binding of acetyl-CoA followed by weak and transient interaction with histone substrate, which permits acetyl transfer. The p300/CBP mechanism differs from that of another family of HATs, PCAF/GCN5 (Poux et al., 2002), which use a ternary complex mechanism.

The p300 HAT/Lys-CoA crystal structure affords the opportunity for computational docking of novel inhibitory scaffolds. In this regard, recent virtual ligand screening based on the X-ray structure of serotonin N-acetyltransferase (AANAT) complexed to a bisubstrate analog led to the identification of a novel, moderately potent and selective small molecule inhibitor for this circadian rhythm enzyme (Szewczuk et al., 2007). In this study, we have pursued the use of this Lys-CoA/p300 HAT structure in virtual ligand screening to identify novel small molecule p300 HAT inhibitors. Below, we describe an in silico search and experimental validation that has led to a commercially available, selective, submicromolar small molecule p300 HAT inhibitory agent with pharmacologic potential.

RESULTS

Ranking and Selection of Compounds from Virtual Screening of the p300 HAT

Compounds from a screening set of nearly 500,000 commercially available small molecules were docked into the p300 HAT structure in the Lys-CoA binding pocket and assigned a score using the ICM-VLS software version 3.5. The components of the ICM (internal coordinate mechanics) score include the internal force-field energy of the ligand, conformational entropy loss of the ligand, receptor-ligand hydrogen-bond interaction, solvation electrostatic energy change, hydrogen-bond donor/acceptor desolvation, and hydrophobic energy (Totrov et al., 1999). The score is trained to separate binders and nonbinders and to rank the interaction of the compound with the receptor. The best score from each of the three docking runs was recorded. The screened compounds were then ranked by ICM score and the 194 highest-scoring compounds (representing 0.04% of the total compound database) were visually inspected and selected based on their availability and interactions with the receptor. Each of the 194 compounds was purchased from ChemBridge and tested experimentally as described below.

Experimental p300 HAT Assays and Inhibitor Validation

After completing the computational docking screen, we tested the top 194 inhibitors of the p300 HAT by employing a convenient

spectrophotometric assay (Kim et al., 2000) followed by a series of secondary assays (see Table S1 available online). In the coupled spectrophotometric assay, the acetyltransferase reaction product CoASH becomes a substrate for alpha-ketoglutarate dehydrogenase, which converts NAD to NADH, resulting in an increase of UV absorbance at 340 nm (Kim et al., 2000). Screening conditions for these p300 assays included semisynthetic HAT enzyme (Thompson et al., 2004), substrate concentrations of 200 μM histone H4-15 peptide and 50 μM acetyl-CoA, and potential small molecule inhibitors tested at 100 μM. Thirty of the original 194 compounds showed at least 50% inhibition under these conditions. To distinguish inhibitory effects related to blockade of coupling enzyme rather than p300, assays were repeated using increased (2-fold) alpha-ketoglutarate dehydrogenase. This eliminated 6 of the 30 hits. To test for protein aggregation-related inhibitory phenomena (Feng et al., 2005), assays with the remaining compounds were next performed in the presence of 0.01% Triton X-100, which attenuated inhibition of eleven of 24 compounds. Nuclear magnetic resonance (NMR) and mass spectrometry confirmed the structure and purity of the 13 potential p300 inhibitors that were subsequently tested in a direct, radioactive assay for IC_{50} measurements. In this radioactive p300 HAT assay, ^{14}C transfer from ^{14}C-acetyl-CoA into peptide substrate is directly measured using Tris-Tricine SDSPAGE and phosphorimage analysis. Three compounds, C646 (ChemBridge#5838646), C146 (ChemBridge#5202146), and C375 (ChemBridge#6643375), were ultimately shown to be relatively potent p300 HAT inhibitors (K_i < 5 μM) (Figure 1A). Interestingly, though C646, C146, and C375 possess distinct scaffolds, these three compounds all contain a linear arrangement of three or four aromatic rings terminating in a benzoic acid.

Acetyltransferase Inhibitor Selectivity

Each of the three inhibitors, C646, C146, and C375, was further analyzed versus other acetyltransferases for specificity (Table S2). We looked at serotonin N-acetyltransferase (Szewczuk et al., 2007), PCAF histone acetyltransferase (Lau et al., 2000a), GCN5 histone acetyltransferase (Poux et al., 2002), Rtt109 histone acetyltransferase (Tang et al., 2008), Sas histone acetyltransferase (Shia et al., 2005), and MOZ histone acetyltransferase (Holbert et al., 2007). Although compound C646 at 10 μM was highly selective in inhibiting p300 (86% inhibition) versus the other six acetyltransferases (less than 10% inhibition), C146 and C375 were less selective, inhibiting at least one of these enzymes with comparable potency to their p300 blockade (Table S2). Thus, compound C646 looked most promising for applications requiring selective inhibition of p300/CBP.

Mechanism of p300 Inhibition

We evaluated the steady-state kinetic mechanism of inhibition of p300 by compounds C646, C146, and C375 by exploring inhibitory effects over a range of acetyl-CoA concentrations. Compounds C646 proved to be a linear competitive inhibitor of p300 versus acetyl-CoA with a K_i of 400 nM (Figure 1B). Compound C146 showed pseudocompetitive inhibition versus acetyl-CoA with K_i-slope = 4.7 μM, although this compound exhibited a measurable K_i-intercept (35 μM), suggesting that C146 still had affinity for the acetyl-CoA-bound form of p300
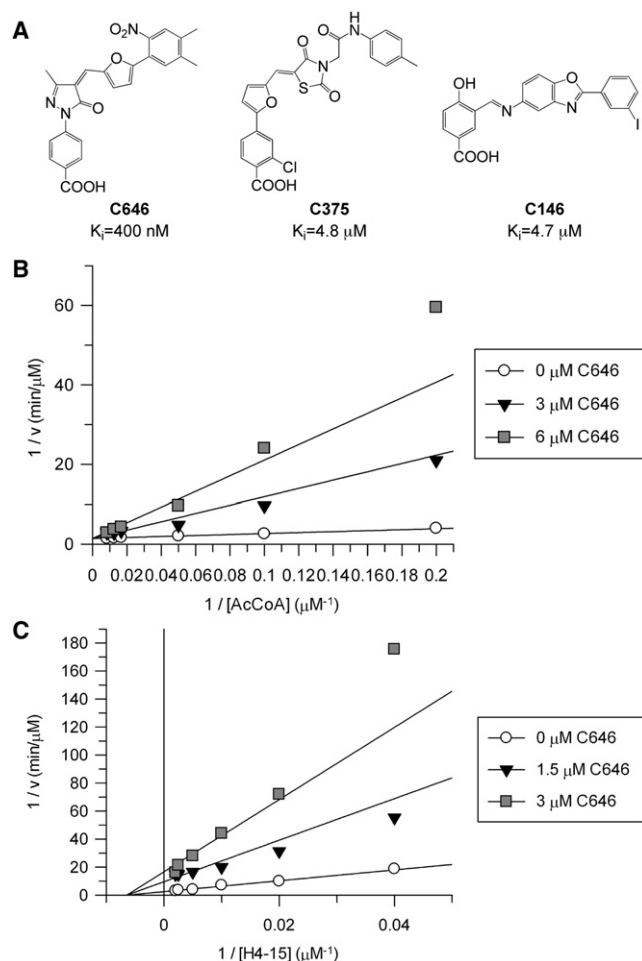
Figure 1. Small Molecule p300/CBP HAT Inhibition and C646 Analysis

(A) Three validated p300 HAT small molecule inhibitors C646, C375, and C146 and their inhibitory constants measured as described in B and Figure S1.

(B) Inhibitory characteristics of C646 toward p300. (A) Plot of $1/v$ versus $1/[\text{acetyl-CoA}]$ at fixed H4-15 peptide substrate (100 μM) and three concentrations of C646 shows competitive inhibition. C646 K_i = 400 ± 60 nM, apparent acetyl-CoA K_m = 8.5 ± 1.4 μM, apparent k_{cat} = 18 ± 1 min^{-1}.

(C) Plot of $1/v$ versus $1/[\text{peptide substrate (H4-15)}]$ at fixed acetyl-CoA (10 μM) and three concentrations of C646 shows noncompetitive inhibition. C646 K_i = 530 ± 40 nM, apparent H4-15 K_m = 155 ± 19 μM, apparent k_{cat} = 40 ± 2 min^{-1}.

(Figure S1A) (Copeland, 2000). C375 showed classical noncompetitive inhibition versus p300 (K_i = 4.8 μM), indicating that it could bind efficiently to the acetyl-CoA bound form of p300 (Figure S1B). Computational models of the complex of these compounds bound to p300 show extensive overlap with the CoA-p300 interaction, so we predicted that a pure competitive kinetic model would be observed. This was only true for C646. In further analysis, compound C646 showed a noncompetitive pattern of p300 inhibition versus H4-15 peptide substrate (Figure 1C), consistent with the expected behavior of a bisubstrate analog interacting with an enzyme with ordered substrate binding, like that of p300 (Yu et al., 2006). Compound C146 was

found to be a competitive inhibitor of p300 versus H4-15 peptide substrate (Figure S1C), suggesting a more complex mode of interaction with the enzyme than a simple bisubstrate analog.

C646 Is Not a Time-Dependent Inactivator of p300

The conjugated pyrazolone exomethylene vinyl functionality in C646 appeared to us to be potentially electrophilic, serving as a possible Michael acceptor, which could covalently modify its protein target. The nucleophilic compound dithiothreitol (DTT) was added to p300 HAT assays, and we showed that C646 inhibitory potency was similar (within 2-fold) if DTT was replaced with beta-mercaptoethanol or glutathione. We investigated whether DTT or beta-mercaptoethanol could generate adducts with C646, however NMR and chromatography revealed no evidence of reaction under the buffer conditions of the enzyme assay. We deduce that this resistance to thiol adduct formation results from the extended conjugation of the polyaromatic system in C646.

Irreversible enzyme inhibitors typically exhibit time-dependent enzyme inactivation (Copeland, 2000; Kitz and Wilson, 1962). In contrast, acetyl transfer catalyzed by p300 HAT in the presence of C646 remained linear over time, consistent with the behavior of a reversible inhibitor (Figure S2A). Moreover, incubation of C646 with p300 for 2, 4, 6, 8, or 10 min prior to acetyltransferase assays showed that the level of inhibition was independent of preincubation time (Figure S2B). Taken together, these results suggest that C646 is a classical reversible p300 inhibitor, consistent with the steady-state kinetic analysis described above.

Conformational Analysis of C646

Prior studies suggested that pyrazolone-furan compounds such as C646 could exist in two double bond stereoisomers involving the exomethylene (Moreau et al., 2008) (Figure S3A). Because the computational docking model of C646 bound to p300 suggests that the compound binds as the Z-isomer, we investigated C646 stereochemistry in solution using ^{1}H NMR and high-pressure liquid chromatography (HPLC). ^{1}H NMR analysis of C646 in dimethyl sulfoxide (DMSO) suggests a 70:30 Z:E-mixture of the olefinic isomers based on the pyrazolone methyl protons (Figure S3A). Using ^{1}H-^{1}H 2D nuclear Overhauser enhancement spectroscopy (NOESY), the major peak can be assigned as the Z-isomer based on the NOE between the vinyl proton and methyl protons in the Z-isomer.

We also show that these isomers can be separated by reverse-phase HPLC (Figure S3B) but that they facilely interconvert, since re-injection of samples derived from the individual peaks shows that re-equilibration of peaks is established within a few hours. These data suggest that the Z-isomer is readily accessible and likely to be favored in solution.

Exploring the Interactions of C646 and p300 Using Site-Directed Mutagenesis

While we have not yet been successful in obtaining an X-ray structure of C646 complexed to p300 HAT, we have used site-directed mutagenesis to evaluate specific interactions predicted by the computational model. In this model, a series of hydrogen bonding donor interactions from the side chains of Thr1411, Tyr1467, Trp1466, and Arg1410 to oxygen atoms of C646 are proposed (Figure 2A). These side chains also make interactions
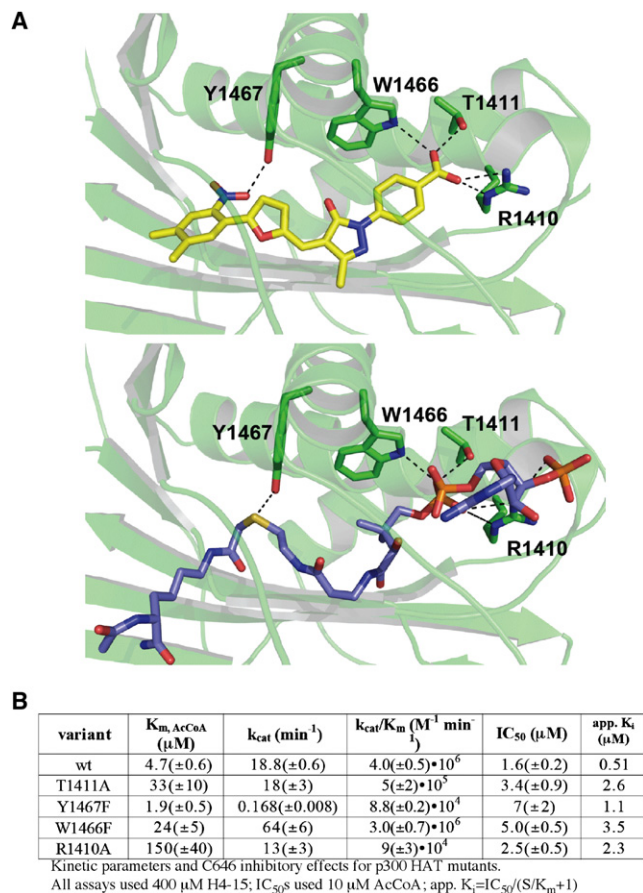
B

variant	$K_{m, AcCoA}$ (μM)	k_{cat} (min^{-1})	k_{cat}/K_m (M^{-1} min^{-1})	IC$_{50}$ (μM)	app. K_i (μM)
wt	4.7($\pm$0.6)	18.8($\pm$0.6)	4.0($\pm$0.5)$\cdot$10^6	1.6($\pm$0.2)	0.51
T1411A	33($\pm$10)	18($\pm$3)	5($\pm$2)$\cdot$10^5	3.4($\pm$0.9)	2.6
Y1467F	1.9($\pm$0.5)	0.168($\pm$0.008)	8.8($\pm$0.2)$\cdot$10^4	7($\pm$2)	1.1
W1466F	24($\pm$5)	64($\pm$6)	3.0($\pm$0.7)$\cdot$10^6	5.0($\pm$0.5)	3.5
R1410A	150($\pm$40)	13($\pm$3)	9($\pm$3)$\cdot$10^4	2.5($\pm$0.5)	2.3

Kinetic parameters and C646 inhibitory effects for p300 HAT mutants.
All assays used 400 μM H4-15; IC$_{50}$s used 10 μM AcCoA; app. K_i=IC$_{50}$/(S/K$_m$+1).

Figure 2. Interactions of C646 with p300

(A) In silico model of C646 bound to p300 HAT active site (upper) shows over-lapping interactions with the X-ray crystal structure of p300 HAT complexed with Lys-CoA (lower).
(B) Kinetic analysis of selected active site mutants.

proteins and used the equation $K_i = IC_{50}/(S/K_m+1)$ to calculate the apparent K_i values based on a competitive inhibition model (Copeland, 2000). As shown in Figure 2B, each mutation increased the apparent K_i of C646 by at least 2-fold, and the most significant effect was seen with W1466F, which showed a 7-fold increase in K_i. This increase may reflect a combination of the loss of the hydrogen bond from the indole nitrogen as well as altered van der Waals contacts. It is noteworthy that the k_{cat}/K_m for W1466F p300 is essentially identical to the wild-type enzyme (Figure 2C), suggesting that inhibition by C646 and catalysis rely on subtly different forces.

Structure-Activity Relationship Analysis of C646 in p300 Inhibition

To explore structural elements of C646 responsible for inhibition of p300, we developed modular synthetic approaches to a series of analogs that could probe the benzoate, pyrazolone, exo-methylene, and arylnitro moieties (see Figure 3; Supplementary Schemes 1-9). The general synthetic approach to prepare many of these analogs involved initially producing the building block phenyl-pyrazolones (**3**) and the aryl-furan aldehydes (Figure 3). Production of the phenyl-pyrazolones (**3**) (Kim and Lee, 1991) was achieved from the corresponding anilines **1**, which could be diazotized and transformed to the aryl hydrazines (**2**). Reaction of intermediates **2** with ethyl acetylacetate led to pyrazo-lones (**3**) formation. Palladium-catalyzed Suzuki coupling of 5-formyl-2-furanboronic acid with aryl halides (**4**) led to aryl-furan aldehydes (**5**) (Langner et al., 2005; Hosoya et al., 2003). Knoeve-nagel condensation between **3** and **5** generated the desired analogs of C646 (Vasyunkina et al., 2005).

Each of the analogs **6a-r** along with two other related commer-cially available derivatives were tested for p300 HAT inhibition using the direct, ^{14}C-acetyl-CoA transfer assay at a range of concentrations and the relative IC$_{50}$s are shown in Figure 4. Derivatization of the carboxylic acid of C646 as the methyl ester affording **6h** led to a dramatic weakening of inhibitory potency (>15-fold), establishing the likely importance of this functionality in hydrogen bonding. Reduction of the C646 enone with sodium borohydride gives rise to C37 (**6c**) and this compound did not detectably block p300 HAT activity (Figure 4). The loss of inhib-itory potency of C37 suggests that shape (planarity) and/or elec-tronic properties of the conjugated system in C646 is critical. Replacement of the C646 nitro group with hydroxymethylene
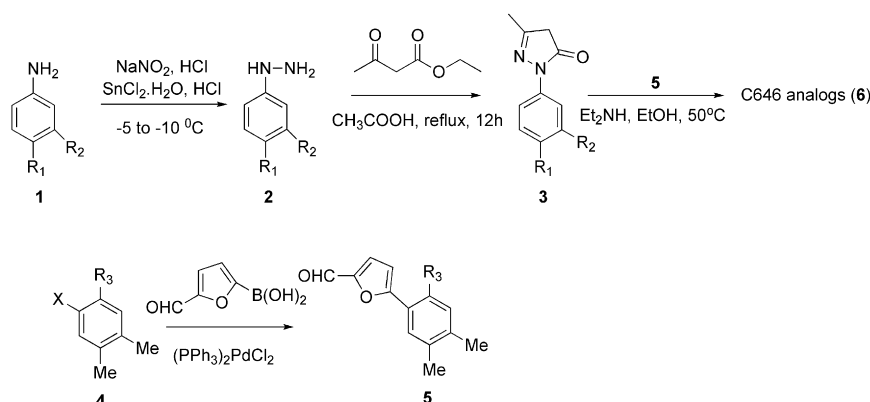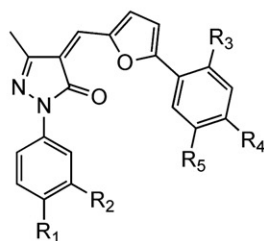
with Lys-CoA based on the X-ray structure (Figure 2A) (Liu et al., 2008a). We thus tested C646 against p300 HAT mutants T1411A, Y1467F, W1466F, and R1410A and the corresponding IC$_{50}$ values are shown in Figure 2B. Because each of these mutants can alter acetyl-CoA interactions as well, we measured the corresponding K_ms for acetyl-CoA for the four mutant

Figure 3. Synthetic Approach to Many of the C646 Analogs in Figure 4

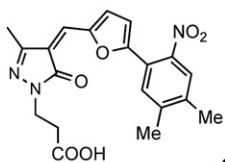More detailed synthetic schemes are shown in the Supplemental Information (Schemes S1-S9).

Figure 4. Synthetic Analogs of C646 and Their Relative IC_{50}s for p300 Inhibition Referenced to C646

Cpd.	R1	R2	R3	R4	R5	IC_{50} relative to C646
C646 (6d)	CO_2H	H	NO_2	Me	Me	1
6f	SO_3H	H	NO_2	Me	Me	0.8
6e	H	CO_2H	NO_2	Me	Me	1
6m	CO_2H	H	CO_2Me	Me	Me	1.3
6o	CO_2H	H	CN	Me	Me	1.7
6a	$CONH_2$	H	NO_2	Me	Me	1.8
6n	CO_2H	H	CO_2Et	Me	Me	1.9
C174	CO_2H	H	NO_2	H	Me	2
6g	SO_2NH_2	H	NO_2	Me	Me	2.1
6i	H	CO_2Me	NO_2	Me	Me	2.4
6b	$CONH_2$	Cl	NO_2	Me	Me	2.6
6j	CONHMe	H	NO_2	Me	Me	3.5
C730	CO_2H	H	F	H	H	6.5
6l	CO_2H	H	CH_2OH	Me	Me	7.7
6h	CO_2Me	H	NO_2	Me	Me	>15

kinetic advantages for in vivo studies (Hodgkiss et al., 1991). However, replacement of the nitrophenyl ring with a pyridine ring (**6p**) eliminated p300 inhibitory action.

Replacing the pyrazolone of C646 with a succinimide ring in the context of a methyl benzoate substituent replacing the nitro group (**6r**) retains potency for p300 inhibition (Figure 4). We have found that a propionate group (**6k**) cannot successfully replace the benzoate ring of C646 and still retain p300 inhibitory potency. Interestingly, carbonyl substitution of the exomethylene vinyl (**6q**) shows 6-fold weaker potency compared with C646.

Effects of C646 on Histone Acetylation in Mouse Cells

We next investigated the effects of compound C646 on cellular histone acetylation using C3H 10T1/2 mouse fibroblasts. We examined histone acetylation using modification-specific antibodies against H3K9ac and H4K12ac (Figure 5). In addition to analysis of total acetylation levels by western blots of SDS gels (Figure 5A) we used acid-urea (AU) gels (Figure 5B) which separate histones on the basis of charge. Loss of a positive charge upon lysine acetylation retards migration, producing a ladder of bands corresponding to integral changes in acetylation (Shechter et al., 2007).

In control cells, basal acetylation levels of H3 and H4 are slightly diminished by C646 treatment over the 1-3 hr time-course tested (Figures 5A and 5B; lanes 1-4). To further investigate this effect, we used a 30 min treatment with the HDAC inhibitor trichostatin A (TSA; Yoshida et al., 1990), which produces increased H3 and H4 acetylation, visualized by the appearance of higher migrating forms in AU gels (Figures 5A and 5B; compare lanes 1 and 5). At all time points tested (1-3 hr; lanes 6-8), incubation with 25 μM C646 prior to addition of TSA virtually completely inhibits this inducible acetylation, both in SDS and AU gels.

By contrast 3 hr treatment with the C646 analog C37, which is devoid of p300 HAT inhibitory activity in vitro, produces no effect on acetylation of H3 or H4 (Figures 5A and 5B; lanes 9, 10). Thus, blockade of p300/CBP by C646 treatment of intact cells results in inhibition of both basal and TSA-inducible acetylation of histones H3 and H4, demonstrating its efficacy in live cells.

(**6l**) also led to a substantial reduction in potency, supporting the importance of hydrogen bonding of the nitro predicted by the computational model.
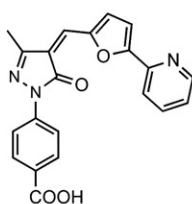
Other hydrogen bond acceptors replacing the C646 para-carboxylic acid were well tolerated at both the para and meta positions including a para-carboxamide (**6a**), a para-sulfonic acid (**6f**), a para-sulfonamide (**6g**), and a meta-methyl ester (**6i**) or carboxylic acid (**6e**). Molecular modeling reveals considerable p300 active-site flexibility in accommodating these other para- and meta-substituted compounds (Figure S4). Molecular recognition versatility with regard to nitrophenyl interactions is indicated by the fact that replacement of the nitro group by methylbenzoate (**6m**) or cyanophenyl (**6o**) functionalities is also well tolerated (Figure 4). That the nitrophenyl group could be effectively replaced by a methylbenzoate might offer pharmaco-
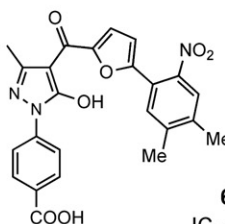
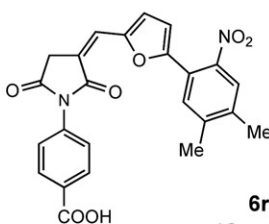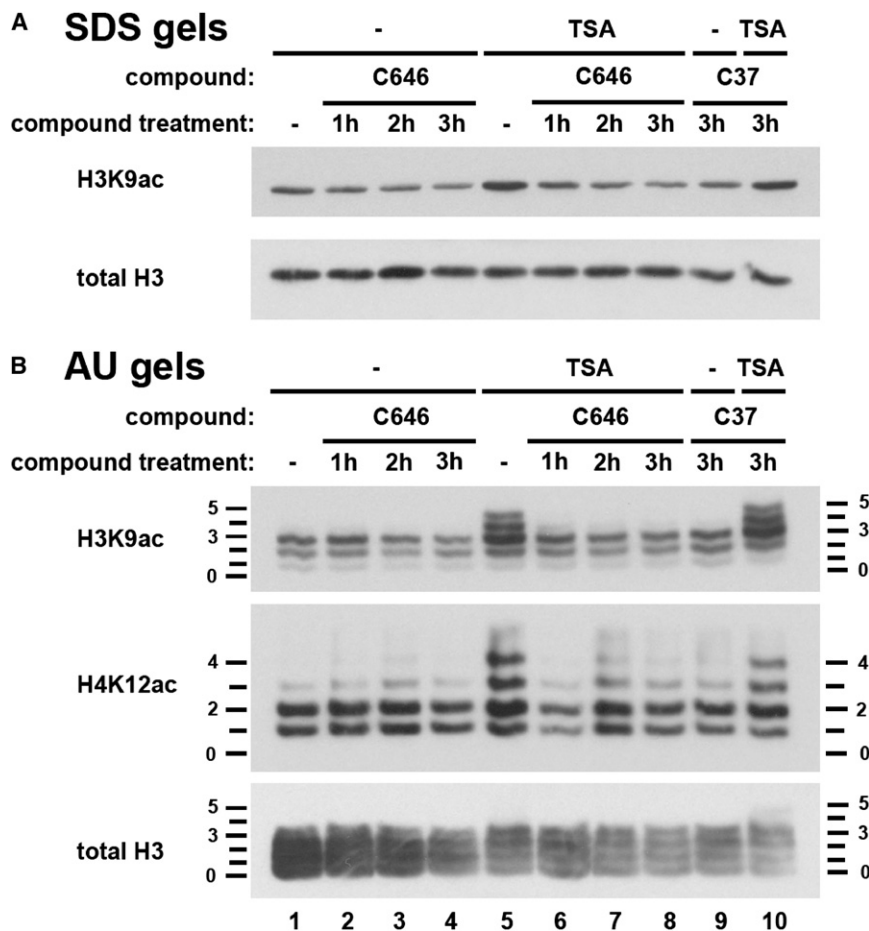**Figure 5. C646 Treatment Reduces Histone H3 and H4 Acetylation Levels and Abrogates TSA-Induced Acetylation in Cells**

Quiescent C3H 10T1/2 mouse fibroblasts were pretreated with C646 (25 μM, lanes 2-4, 6-8) for the indicated times (1, 2, or 3 hr) or the control compound, C37 (25 μM, 3 hr, lanes 9, 10), and TSA (33 nM) added where indicated (lanes 6-8, 10) for the final 30 min of incubation. Histones were extracted and analyzed by western blotting to visualize total H3 and H3K9ac using SDS (A) or H3, H3K9ac, and H4K12ac using acid-urea (B) gel electrophoresis. Acid-urea gels separate histones on the basis of charge. Each acetylation event incrementally retards migration to produce a "ladder" of bands, numbers on either side of the blot indicating extent of modification (lane 1, untreated control cells; lane 5, TSA-treated cells).

Similar inhibition was observed in cells subject to RNA interference targeting this enzyme (N.T.C., C.A.H., E.M.B., R.M.A., and L.M., unpublished data).

Cell Growth Effects of C646 on Melanoma and Lung Cancer Lines

Given the broad and important effects of p300/CBP on key genes and pathways involved in cell growth, we explored the pharmacologic effects of C646 on ^{3}H-thymidine incorporation at 24 hr in three melanoma (Figure 6A) and three non-small-cell lung cancer lines (Figure 6B). We compared the effects of C646 (10 μM) and the peptide-based bisubstrate p300/CBP HAT inhibitor Lys-CoA-Tat (25 μM) and found that both were capable of reducing ^{3}H-thymidine incorporation in several of these human cancer lines to varying degrees (Figures 6A and 6B). Control compounds, C37 and Ac-DDDD-Tat, which lack p300 inhibitory properties, had no effects on ^{3}H-thymidine incorporation as shown in Figures 6A and 6B. In general, reduction of ^{3}H-thymidine incorporation was correlated for Lys-CoA-Tat and C646 among the different cell lines (Figures 6A and 6B), consistent with a common protein target presumed to be the p300/CBP HAT, although C646 generally showed greater effects at the doses used. For example, the melanoma line WM35 and the lung cancer line H23 were quite susceptible to C646 treatment, with Lys-CoA-Tat, showing modest inhibitory effects in these cells. Notably, the immortalized murine fibroblast

cell line, NIH 3T3, was not inhibited by C646 at 20 μM, suggesting a differential effect on the malignant cells evaluated (Figure 6C).

We pursued more detailed studies on the moderately sensitive melanoma line WM983A and showed that the IC$_{50}$ for C646 was in the range of 10-20 μM, but that this cell line was resistant to the C646 analog control compound C37 at 20 μM (Figure 7A). Correlating with this growth effect on WM983A cells was a dose-dependent reduction in global histone H3 acetylation revealed by western blotting that were treated for 6 hr (Figure 7B). Based on fluorescence-activated cell sorting (FACS) analysis, the effects of C646 (20 μM, 24 hr treatment) on WM983A and the more sensitive melanoma line WM35 were consistent with a G1-S cell cycle arrest, predicted to be related to p300 modulation (Iyer et al., 2007), because the S-phase dropped under these conditions (Figure 7C).

DISCUSSION

This study has led to the identification of a relatively potent and selective small molecule p300 HAT inhibitor, which was discovered by using virtual ligand screening. The docking model used the ICM approach, which has been successful in identifying ligands for a range of other protein targets (Szewczuk et al., 2007; Mallya et al., 2007; Bisson et al., 2009; Cavasotto et al., 2008). An X-ray crystal structure of the complex of p300 HAT with the bisubstrate analog Lys-CoA revealed a pocket that included a series of hydrogen bonding residues that interact with the pantetheine moiety of Lys-CoA as well as two phosphate groups. The pyrazolone C646 was predicted to dock into this site, utilizing several of the same residues. Such active site interactions between C646 and p300 were projected to result in exclusion of acetyl-CoA. Consistent with this model, C646 was a competitive p300 inhibitor versus acetyl-CoA using steady-state kinetic analysis. No evidence of time-dependent
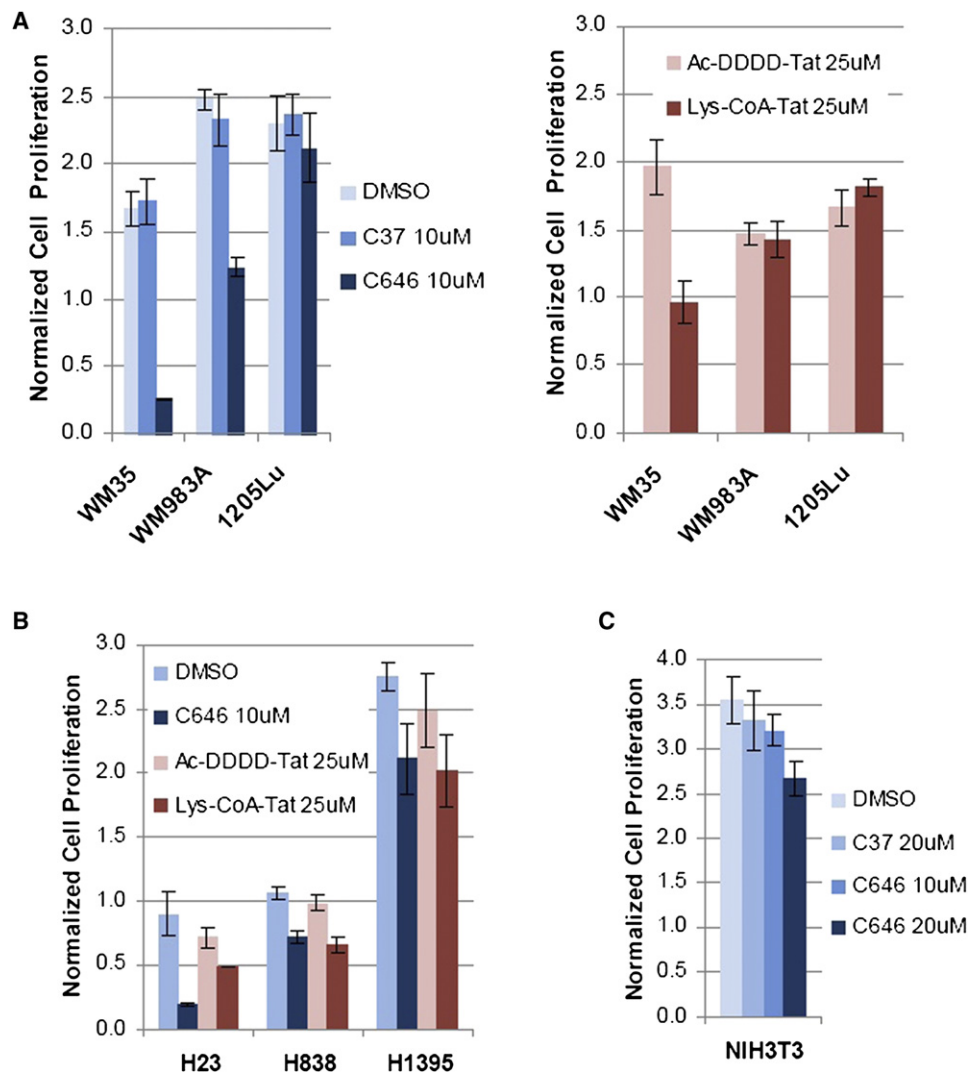
Figure 6. p300/CBP HAT Inhibitors and Cell Growth Effects

(A) C646 has a more potent effect on cell growth than Lys-CoA-Tat does. Cells were treated for 24 hr and proliferation was measured via ^{3}H-thymidine incorporation pre- and posttreatment. Data for each cell line were normalized to ^{3}H counts measured pretreatment. C37 is an inactive derivative of C646. DMSO serves as a vehicle control for C37 and C646. Ac-DDDD-Tat is a control peptide for Lys-CoA-Tat. WM35, WM983A, and 1205Lu are melanoma cell lines representing three stages of cancer progression: radial, vertical, and metastatic, respectively.

(B) Two out of three non-small-cell lung adenocarcinoma cell lines demonstrate significant growth inhibition after treating with C646 and Lys-CoA-Tat for 24 hr.

(C) C646 does not have a significant inhibitory effect on NIH 3T3 cell proliferation.

inactivation of p300 by C646 was observed, arguing against the idea that C646 was undergoing covalent reaction with the enzyme. For an ordered binding mechanism like p300s, bisubstrate analogs are predicted to be noncompetitive inhibitors versus the second substrate, as found for C646.

The nature of the interaction between C646 and p300 was also probed by altering enzyme residues and functional groups in the inhibitor. These studies showed a maximal effect of a 7-fold drop in affinity by mutagenesis of Trp1466 to Phe in p300 and > 15-fold effects for several synthetic modifications of C646. Taken together, these results further support active site targeting of p300 by C646, although ultimately an X-ray crystal structure of the complex will be needed to most rigorously test the computa-

tional model proposed. The relative resistance of the W1466F p300 mutant to C646 but the retention of wild-type catalytic activity suggest that it may ultimately be possible to pursue chemical-genetic complementation studies on p300/CBP analogous to those done on protein kinases (Shogren-Knaak et al., 2001; Qiao et al., 2006).

Compound C646 appears selective versus the other acetyltransferases so far examined. Compared with HDACS, HATs show greater sequence and structural divergence and specific targeting is more tractable (Hodawadekar and Marmorstein, 2007; Haberland et al., 2009; Cole, 2008). Although p300 and Rtt109 are similar in fold, these two proteins show very little or no sequence homology to other HATs and very modest
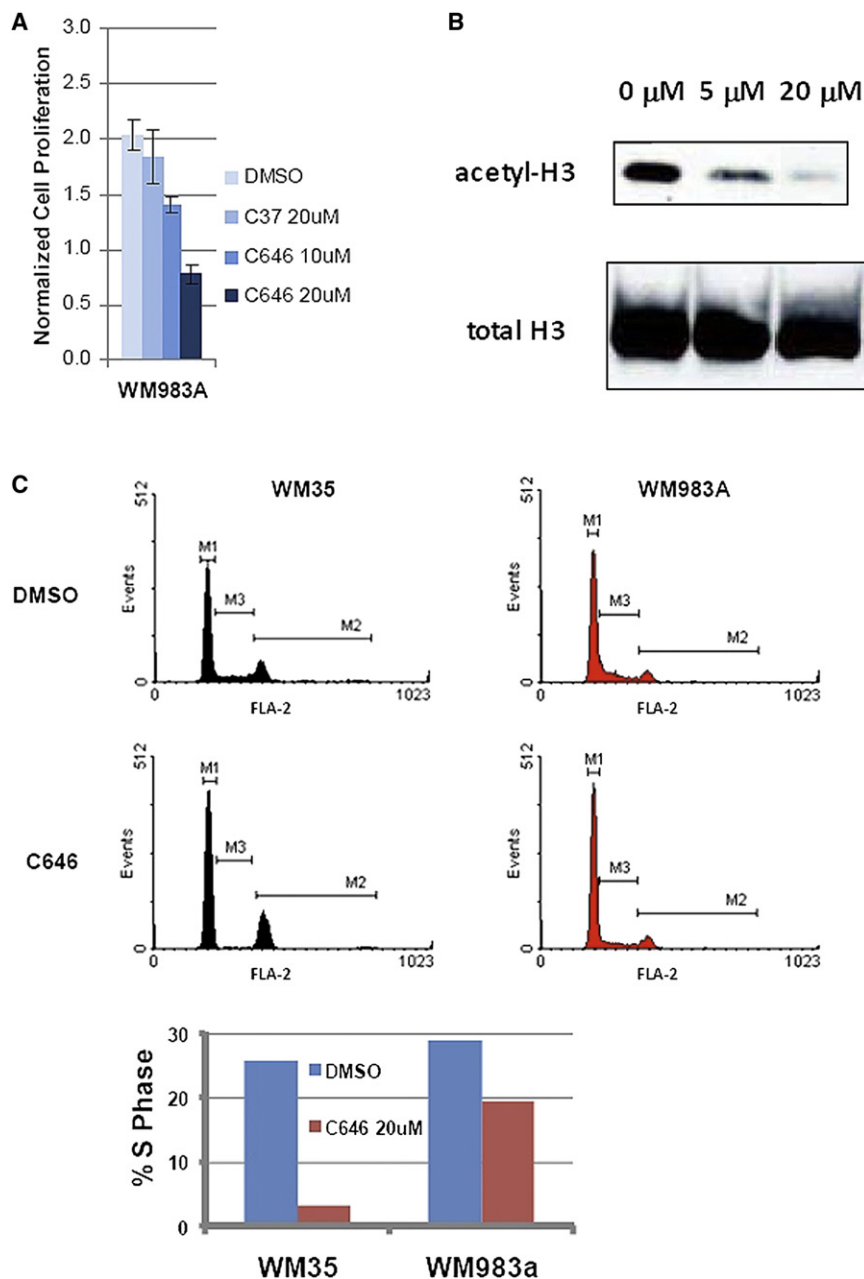
Figure 7. C646 Inhibits Histone Acetylation in Melanoma and Confers G1-S Phase Cell Cycle Blockade

(A) C646 inhibits WM983A melanoma cell proliferation but C37 does not. Cells were treated with each compound for 24 hr. Proliferation was measured via ^{3}H-thymidine incorporation.

(B) C646 blocks H3 acetylation in WM983A cells. Cells were treated for 6 hr with increasing concentrations of C646. Nuclear lysates were subjected to western blot analysis for acetylated H3 (Upstate 06-599). Total H3 (Abcam ab1791) was blotted as a loading control.

(C) C646 causes growth arrest in melanoma cell line WM35 and WM983A, indicated by a decrease in %S phase. Cells were treated for 24 hr with 20 μM C646 or DMSO, then collected and stained with propidium iodide, followed by FACS analysis.

nonspecific or are predicted to be quite chemically reactive, limiting their utility (Stimson et al., 2005; Balasubramanyam et al., 2003; Balasubramanyam et al., 2004; Ravindra et al., 2009). Lys-CoA is 20-fold more potent than C646 but is not cell permeable. Lys-CoA-Tat is more potent in vitro than C646 but is apparently also less active in cells and is a much more complicated molecule to make and work with.

Virtual ligand screening offers a relatively rapid, economical approach to search for potent enzyme inhibitors. The complexity of coping with solvation and conformational changes in proteins and estimating energetics of atomic interactions makes small molecule in silico docking a continuing challenge. Indeed, only three of the top 194 computational p300 ligands were confirmed to be reasonably potent inhibitors and only one proved competitive versus acetyl-CoA as predicted. It is generally understood that the virtual screening against one of even several conformations of the binding pocket is not designed to identify all potential p300/CBP inhibitors because the conformations of the binding pocket for certain chemical classes of inhibitors may extend far beyond the pocket conformation we used. Nevertheless, we suspect that even identifying one relatively potent and selective active site compound for p300 out of 194 experimentally tested compounds represents a higher ratio of success than expected from a high-throughput screen of unselected small molecule libraries (Stimson et al., 2005).

We have also shown that C646 works rapidly in cell culture in blocking histone acetylation. The application of selective p300/CBP HAT inhibitors in vivo can help address a range of biological and pathophysiologic questions.

structural detailed homology in active-site interactions (Wang et al., 2008). Moreover, the GNATs PCAF and serotonin N-acetyltransferase and the MYST family member MOZ make distinctive three-dimensional interactions with CoA (Hodawadekar and Marmorstein, 2007).

The most potent and selective small molecule p300/CBP HAT inhibitor prior to this study is a garcinol derivative, LTK14, with a K_i of 5.1 μM (Mantelingu et al., 2007; Arif et al., 2009), about 12-fold weaker than C646. The complex natural product analog LTK14 is suggested to be a noncompetitive p300 inhibitor versus both acetyl-CoA and peptide and the structural basis of inhibition remains uncertain (Arif et al., 2009). Other published, small molecule p300 inhibitors including anacardic acid, curcumin, plumbagin, and isothiazolones have been demonstrated to be

SIGNIFICANCE

HDAC inhibitors, despite their limited selectivity, have been enormously important in dissecting the role of histone acetylation in gene expression pathways, and SAHA is clinically used for cancer treatment (Itoh et al., 2008). Our data here with the relatively potent, selective p300/CBP inhibitor C646 indicate the potential of p300/CBP HAT blockade in impeding cancer proliferation, though more work will be needed to clarify the multiple potential mechanisms for such growth effects. Other recently published studies underscore the potential value of blocking p300/CBP HAT in the treatment of diabetes mellitus, cardiac disease, and HIV (Cole 2008).

EXPERIMENTAL PROCEDURES

Molecular Modeling

The crystal structure of p300 HAT in complex with bisubstrate analog Lys-CoA (Protein Data Bank ID 3BIY) was prepared for virtual screening using the Internal Coordinate Mechanics (ICM-Pro) software version 3.5 (MolSoft LLC, San Diego CA) (Abagyan et al., 1994). The ligand and heteroatom molecules were removed from the structure and a continuous dielectric was used in place of the water molecules. Missing hydrogen and heavy atoms were added and atom types and partial charges were assigned. The protein model was adjusted so that the optimal positions of polar hydrogens were identified, the most isomeric form of each histidine was assigned and the correct orientation of the side-chains of glutamine and asparagine were found. Steric clashes were removed by an energy minimization procedure.

Virtual Screening

Virtual screening was undertaken with the ICM-VLS software version 3.5 (MolSoft LLC, San Diego, CA) using dockScan version 4.4. This method uses an extension of the Empirical Conformational Energy Program for Peptides 3 (ECEPP/3) (Nemethy et al., 1992) force field parameters for proteins and the Merck Molecular Force Field (MMFF) (Halgren and Nachbar, 1996) for small molecules. Five continuously differentiable potential grid maps were calculated for the receptor using spline interpolation for efficient gradient minimization (Totrov and Abagyan, 1997). These maps include energy terms for electrostatics, directional hydrogen bond, hydrophobic interactions, and two for van der Waals interactions for steric repulsion and dispersion attraction including a soft potential to limit the effect of minor steric clashes. A collection of 492,793 compounds from the ChemBridge small molecule database (ChemBridge Corp, San Diego, CA) was screened to the p300 HAT bisubstrate inhibitor binding site. Each ligand was docked into the binding pocket three times. During docking the ligand is flexible and its position and internal torsions are sampled using the ICM biased probability Monte Carlo procedure, which includes a local minimization after each random move. Each docked ligand is assigned a score according to the weighted components of the ICM-VLS scoring function (Totrov and Abagyan, 1999).

Peptide Synthesis

Synthetic peptides (H4-15, p300 peptides, Lys-CoA-Tat, Ac-DDDD-Tat) were prepared using automated solid phase peptide synthesis and the Fmoc strategy as described previously (Thompson et al., 2001; Zheng et al., 2005; Guidez et al., 2005; Liu et al., 2008a, 2008b). Peptides were purified using reverse-phase HPLC and their structures confirmed by mass spectrometry.

Purification of Semisynthetic p300 HAT Domain

A variant of the HAT domain of p300 (residues 1287 to 1652) was expressed as a fusion with the VMA intein chitin binding domain as described previously (Thompson et al., 2004). Residues 1529-1560, comprising the regulatory autoacetylation loop, were deleted in the construct, rendering the enzyme constitutively active. The construct also contained an M1652G mutation. *E. coli* BL21(RIL)-DE3 cells containing the construct were grown to OD_{600} of 0.6 at 37°C. The incubator was cooled to 16°C, and expression was induced by addition of 500 μM IPTG. Following overnight expression, the cells were centrifuged and resuspended in lysis buffer prior to lysis via three passes through a French pressure cell. Lysates were clarified through centrifugation and incubated with chitin resin for 30 min at 4°C. The resin was washed thoroughly before addition of 200 mM MESNA and a C-terminal peptide corresponding to residues 1653-1666 of p300. The expressed protein ligation reaction was allowed to proceed for 16 hr followed by purification over a MonoS 5/50 GL strong cation exchange column (GE Healthcare) using linear gradients of NaCl (50 to 1000 mM). Purified semisynthetic p300 was concentrated and dialyzed against 20 mM HEPES (pH 7.9), 50 mM NaCl, 1 mM DTT, and 10% glycerol (v/v) prior to flash-freezing in liquid N_2 and storage at −80°C. Protein concentration was determined by gel and by Bradford assay using bovine serum albumin (BSA) as a standard.

Initial Screen of VLS Hits

The top 194 p300 HAT inhibitor candidates identified by VLS were screened using a coupled spectrophotometric assay. In this assay, CoASH produced by the p300 reaction is used by α-ketoglutarate dehydrogenase (α-KGDH) to produce NADH, which can be monitored spectrophotometrically at 340 nm (Kim et al., 2000). Reactions were performed at 30°C in 1 M HEPES (pH 7.9) and contained 200 μM H4-15, 200 μM TPP, 5 mM $MgCl_2$, 1 mM DTT, 50 μg/mL BSA, 200 μM NAD, 2.4 mM α-ketoglutarate, 200 μM acetyl-CoA, 0.1 units α-KGDH, and 100 nM p300. DMSO was kept at a constant 3.3%, and candidate compounds were screened at 100 μM. Reaction mixtures were incubated at 30°C for 10 min prior to initiation. Reactions were initiated with addition of H4-15 and followed over the linear portion of the progress curve, which provides the initial velocity via linear regression. Percent inhibition was determined by comparison with velocity without candidate added. Compounds that exhibited over 40% inhibition were subjected to further screening steps. To ensure that compounds were not inhibiting α-KGDH instead of p300, compounds were assayed with 0.2 units of α-KGDH, two times the amount used in the initial screen. To ensure that compounds were not inhibiting through nonspecific aggregation, compounds were assayed in the presence of 0.01% Triton X-100. Compounds whose inhibition was greatly decreased either by raising the α-KGDH concentration or by preventing nonspecific aggregation were removed from further consideration.

Compounds that passed the iterative verification process in the initial screen were then tested in a direct radioactive assay. In this assay, production of ^{14}C-labeled Ac-H4-15 is monitored electrophoretically (Thompson et al., 2001). Reactions were performed in 20 mM HEPES (pH 7.9), and contained 5 mM DTT, 80 μM EDTA, 40 μg/ml BSA, 100 μM H4-15, and 5 nM p300. DMSO was kept constant at 2.5%, and inhibitors were screened at 25 μM. Reactions were incubated at 30°C for 10 min, initiated with addition of a 1:1 mixture of ^{12}C-acetyl-CoA and ^{14}C-acetyl-CoA to a final concentration of 20 μM, and allowed to run for 10 min at 30°C. Reactions are then quenched with addition of 14% SDS (w/v). Turnover was kept below 10%. All compounds were screened in duplicate. Samples were then loaded onto a 16% Tris-Tricine gel along with a BSA standard and run at 140 V for 90 min. Gels were washed and dried, and exposed in a PhosphorImager cassette for ~2 days. Bands corresponding to Ac-H4-15 were then quantified using ImageQuant. Compounds exhibiting over 40% inhibition compared to control were then kinetically characterized.

Kinetic Characterization of Verified Inhibitors and Analogs

IC_{50} values for the putative p300 HAT inhibitors identified through the initial screen were determined using the direct radioactive assay described above. Reactions were performed in 20 mM HEPES (pH 7.9), and contained 5 mM DTT, 80 μM EDTA, 40 μg/ml BSA, 100 μM H4-15, and 5 nM p300. Putative inhibitors were added over a range of concentrations, with DMSO concentration kept constant (<5%). Reactions were incubated at 30° for 10 min, then initiated with addition of a 1:1 mixture of ^{12}C-acetyl-CoA and ^{14}C-acetyl-CoA to 20 μM. After 10 min at 30°C, reactions were quenched with 14% SDS (w/v). All concentrations were screened in duplicate. Gels were run, washed, dried, and exposed to a PhosphorImager plate as described above, and production of Ac-H4-15 quantified to obtain IC_{50}s.

Patterns of inhibition of putative p300 HAT inhibitors were determined in a similar fashion. One substrate was held constant while the other was varied over a range of three inhibitor concentrations (0, 0.5 × IC_{50}, and IC_{50}). AcCoA was varied from 5-120 μM while holding H4-15 constant at 100 μM, and H4-15

was varied from 25–500 μM while holding acetyl-CoA constant at 10 μM. Reactions were performed in duplicate as described above; enzyme concentration and reaction time were varied to keep turnover below 10%. Following quantification, data were globally fit to equations for competitive or noncompetitive inhibition to determine the optimal pattern of inhibition (Copeland, 2000).

Determining Inhibitor Specificity for p300 HAT

C646, C375, and C146 were screened spectrophotometrically against PCAF (p300/CBP-associated factor, a histone acetyltransferase) and AANAT (arylalkylamine N-acetyltransferase, a non-histone acetyltransferase) using a similar coupled assay as described above. PCAF reactions were performed in 100 mM HEPES (pH 7.9), and contained 200 μM TPP, 5 mM MgCl₂, 1 mM DTT, 50 mM NaCl, 0.05 mg/ml BSA, 200 μM NAD, 2.4 mM α-KG, 30 μM acetyl-CoA, 0.037 units α-KGDH, 3.3% DMSO, and 10 μM inhibitor. Reactions took place at 30°C. Reactions were initiated by addition of 10 nM PCAF and were followed at 340 nm over the linear portion of the curve below 10% turnover. AANAT reactions were performed in 100 mM NH₄OAc (pH 6.8) and contained 200 μM TPP, 5 mM MgCl₂, 1 mM DTT, 50 mM NaCl, 0.05 mg/ml BSA, 200 μM NAD, 2.4 mM α-KG, 200 μM AcCoA, 0.1 units α-KGDH, 3.3% DMSO, and 10 μM inhibitor. Reactions took place at 25°C. Reactions were initiated with addition of 65 nM AANAT, and followed at 340 nm, as above. Percent inhibition values were compared to those with p300, which were repeated using the protocol given above. C646 was further analyzed as a potential HAT inhibitor with yeast GCN5, the Sas2/4/5 complex, MOZ, and Rtt109. Yeast GCN5, MOZ, and the Rtt109/Vps75 complex were purified as described elsewhere (Poux et al., 2002; Tang et al., 2008; Holbert et al., 2007). The SAS complex was expressed and purified in E. coli as detailed elsewhere (Shia et al., 2005; Sutton et al., 2003). Briefly, the SAS2, SAS4, and SAS5 proteins were coexpressed using the Duet system (Novagen) in BL21-CodonPlus(DE3)-RIL cells (Stratagene). The complex was purified using a combination of nickel affinity, ion exchange (HiTrap SP), and gel filtration (Superdex 200) chromatography.

HAT assays with yeast GCN5, SAS complex, MOZ, and Rtt109/Vps75 complex used the direct radioactive assay described above. Reactions were carried out at 30°C for times varying from 2 to 4 min under the following reaction conditions: 50 mM HEPES (pH 7.9), 50 mM NaCl, 0.05 mg/ml BSA, 5 mM DTT, 0.05 mM EDTA, 0.25% DMSO, 10 μM X. laevis histone H3, and varying concentrations of C646 (0, 3, 10 μM). The reactions contained either 70 ng Rtt109/Vps75, 15 ng yGcn5, 300 ng SAS complex, or 1 μg hMOZ. The amount of enzyme used in each assay was estimated by comparing Coomassie blue staining of samples with BSA standards, analyzed by SDS-PAGE. The mixture was allowed to equilibrate at 30°C for 10 min before the reaction was initialed with addition of a 1:1 mixture of ¹²C-AcCoA and ¹⁴C-AcCoA to a final concentration of 20 μM. After the appropriate time the reaction was quenched with 6 X Tris-Tricine gel loading buffer, which contained 0.2 M Tris-Cl (pH 6.8), 40% v/v glycerol, 14% w/v SDS, 0.3 M DTT, and 0.06% w/v Coomassie blue. The ¹⁴C-labeled histone substrates were separated from reactants on a 16.5% Tris-Tricine SDS-PAGE gel. The rate of ¹⁴C-incorporation into histone H3 was quantified by autoradiography. We performed all assays in duplicate, and these generally agreed within 20%.

Time Course Studies

Time courses of p300 HAT with C646 were determined using the radioactive assay described above. Reactions were performed using the conditions detailed above with 1.5 μM C646. Reactions were quenched at particular time intervals, then run on a 16% Tris-Tricine gel and quantified as described above. Similar studies were performed varying the time of p300 HAT pre-incubation with C646. Assays contained the conditions detailed above, with 1.5 μM C646 added at various times prior to initiation with 10 μM acetyl-CoA. Reactions were quenched after 5 min, then run on a 16% Tris-Tricine gel and quantified as described above. All time points were screened in duplicate.

Inhibition with p300 Mutants

Sites for mutation were chosen by examination of the C646 binding model generated during VLS. T1411A, W1466F, Y1467F, and R1410A mutations were installed using QuikChange protocols. p300 variants were expressed in E. coli BL21(RIL)-DE3 cells and purified using expressed protein ligation as

described above. IC₅₀ values for C646 with all mutants were obtained using the methods described above. All assays contained 10 μM of a 1:1 mixture of ¹²C-acetyl-CoA and ¹⁴C-acetyl-CoA and 400 μM H4-15. Reaction time was varied between 5 and 10 min to keep turnover below 10%. Enzyme concentrations were altered for each mutant, as active site mutations affected enzyme activity. In a similar fashion, kinetic parameters for each mutant versus AcCoA were determined. [H4-15] was 400 μM, and DMSO was held constant at 2.5%. Reactions proceeded for 6 min before being quenched and run on a 16% Tris-Tricine gel as described above. Data were quantified and fit to the Michaelis-Menten equation.

NMR Studies

The 2D ¹H-¹H correlation spectra were acquired at 30°C on an 11.7 T Varian INOVA spectrometer using a pentaprobe equipped with z-axis pulse-field gradient coils.

Data were processed and analyzed using NMRPipe (Delaglio et al., 1995). The sample contained 600 μl 10 mM C646 DMSO-d6 solution.

Histone acetylation assays in mouse cells

C3H 10T1/2 mouse fibroblasts were grown in DMEM with 10% FCS at 37°C with 6% CO₂.

Confluent cultures were rendered quiescent in DMEM with 0.5% FCS for 18-20 hr prior to treatment. Cells were treated with the following compounds: TSA (10 ng/ml [33 nM]; Sigma), C646 (25 μM), C37 (25 μM). Antibodies were used at the following concentrations: total H3 (1:10000; ab7834; Abcam); H4K12ac (1:2500; 06-761; Upstate). Rabbit anti-H3K9ac (1:10000) antibodies were generated in-house (Edmunds et al., 2008). Histones were isolated from cells by acid extraction, separated by SDS and acid-urea polyacrylamide gel electrophoresis and analyzed by western blotting as described previously (Thomson et al., 1999; Clayton et al., 2000).

Cancer Cell Studies

Melanoma cell lines WM35, WM983A, and 1205Lu were generous gifts from Meenhard Herlyn's lab at the Wistar Institute (Philadelphia, PA). Non-small-cell lung cancer (NSCLC) cell lines H23 and H838 were obtained from Dr. Charles Rudin's lab, and H1395 from Dr. Craig Peacock's lab, at Johns Hopkins. Melanoma cells were maintained in Dulbecco's modified Eagle medium. NSCLCs were maintained in RPMI Medium 1640. Both types of media were supplemented with 10% fetal bovine serum (FBS), penicillin-streptomycin, and L-glutamine. Media, pen-strep, and L-glutamine were purchased from Invitrogen. FBS was purchased from Gemini Bio-Products (#100106).

Before treating cells with p300 inhibitors (C646, Lys-CoA-Tat [Zheng et al., 2005; Guidez et al., 2005]) or control compounds (C37, Ac-Asp-Asp-Asp-Asp-Tat [also known as Ac-DDDD-Tat]), cells were plated at sub-confluent concentration (~60%) and incubated at 37°C until attached to the plating surface. Compound stocks (10-20 mM in anhydrous DMSO) were directly added to culture media at desired concentrations. DMSO concentration was kept constant at 0.2% between different treatment conditions. Cells were seeded in 96-well plates at ~5000 cells per well on average, depending on each cell line's doubling time. After attachment, cells were treated with p300 inhibitors, control compounds, or DMSO for 24 hr. After treatment, ³H-thymidine (1 mCi/ml stock) was added to media at 10 μCi/ml final concentration. Cells were incubated for an additional 5 hr, then trypsinized and collected onto a filter mat using a Cell Harvester (PerkinElmer). Radioactivity was measured with a MicroBeta plate reader (PerkinElmer). Each sample was tested in triplicate.

Cell Cycle Analysis

Cells treated with C646 or DMSO were stained with propidium iodide (PI) according to a published protocol (Robinson, 2009). Briefly, equal numbers of cells (greater than 10⁶) in 0.5 ml phosphate-buffered saline (PBS) were fixed in 70% ethanol for at least 2 hr at 4°C. A stock staining solution containing 10 ml 0.1% Triton X-100 in PBS, 400 μl of RNase cocktail (equivalent of ~200 units of RNase A) (Ambion), and 200 μl of 1 mg/ml PI was prepared. Fixed cells were spun at 200 g for 5 min (Beckman Coulter Allegra® X-12R, with an SX4750A rotor), rehydrated in 5 ml PBS, and spun again to remove all traces of ethanol. Cells were stained with 1 ml staining solution for 20 min at 37°C, then immediately analyzed on a FACSCalibur flow cytometer (BD Biosciences) at

the Johns Hopkins Flow Cytometry Core Facility. Data acquisition and analysis were performed with the CellQuest software (BD). WinMDI 2.9 (http://facs.scripps.edu.software.html) was also used for data presentation.

REFERENCES

Abagyan, R., Totrov, M., and Kuznetsov, D. (1994). ICM—a new method for protein modeling and design: applications to docking and structure prediction from the distorted native conformation. J. Comput. Chem. 15, 488–506.

Arif, M., Pradhan, S.K., Thanuja, G.R., Vedamurthy, B.M., Agrawal, S., Dasgupta, D., and Kundu, T.K. (2009). Mechanism of p300 specific histone acetyltransferase inhibition by small molecules. J. Med. Chem. 52, 267–277.

Balasubramanyam, K., Swaminathan, V., Ranganathan, A., and Kundu, T.K. (2003). Small molecule modulators of histone acetyltransferase p300. J. Biol. Chem. 278, 19134–19140.

Balasubramanyam, K., Varier, R.A., Altaf, M., Swaminathan, V., Siddappa, N.B., Ranga, U., and Kundu, T.K. (2004). Curcumin, a novel p300/CREB-binding protein-specific inhibitor of acetyltransferase, represses the acetylation of histone/nonhistone proteins and histone acetyltransferase-dependent chromatin transcription. J. Biol. Chem. 279, 51163–51171.

Bannister, A.J., and Kouzarides, T. (1996). The CBP co-activator is a histone acetyltransferase. Nature 384, 641–643.

Bisson, W.H., Koch, D.C., O'Donnell, E.F., Khalil, S.M., Kerkvliet, N.I., Tanguay, R.L., Abagyan, R., and Kolluri, S.K. (2009). Modeling of the aryl hydrocarbon receptor (AhR) ligand binding domain and its utility in virtual ligand screening to predict new AhR ligands. J. Med. Chem. 52, 5635–5641.

Cavasotto, C.N., Orry, A.J., Murgolo, N.J., Czarniecki, M.F., Kocsi, S.A., Hawes, B.E., O'Neill, K.A., Hine, H., Burton, M.S., Voigt, J.H., et al. (2008). Discovery of novel chemotypes to a G-protein-coupled receptor through ligand-steered homology modeling and structure-based virtual screening. J. Med. Chem. 51, 581–588.

Choudhary, C., Kumar, C., Gnad, F., Nielsen, M.L., Rehman, M., Walther, T.C., Olsen, J.V., and Mann, M. (2009). Lysine acetylation targets protein complexes and co-regulates major cellular functions. Science 325, 834–840.

Clayton, A.L., Rose, S., Barratt, M.J., and Mahadevan, L.C. (2000). Phosphoacetylation of histone H3 on c-fos- and c-jun-associated nucleosomes upon gene activation. EMBO J. 19, 3714–3726.

Cole, P.A. (2008). Chemical probes for histone-modifying enzymes. Nat. Chem. Biol. 4, 590–597.

Copeland, R.A. (2000). Enzymes: A Practical Introduction to Structure, Mechanism, and Data Analysis, Second Edition (New York: Wiley-VCH).

Dekker, F.J., and Haisma, H.J. (2009). Histone acetyl transferases as emerging drug targets. Drug Discov. Today 14, 942–948.

Delaglio, F., Grzesiek, S., Vuister, G.W., Zhu, G., Pfeifer, J., and Bax, A. (1995). NMRPipe: a multidimensional spectral processing system based on UNIX pipes. J. Biomol. NMR 6, 277–293.

Edmunds, J.W., Mahadevan, L.C., and Clayton, A.L. (2008). Dynamic histone H3 methylation during gene induction: HYPB/Setd2 mediates all H3K36 trimethylation. EMBO J. 27, 406–420.

Feng, B.Y., Shelat, A., Doman, T.N., Guy, R.K., and Shoichet, B.K. (2005). High-throughput assays for promiscuous inhibitors. Nat. Chem. Biol. 1, 146–148.

Goodman, R.H., and Smolik, S. (2000). CBP/p300 in cell growth, transformation, and development. Genes Dev. 14, 1553–1577.

Gu, W., and Roeder, R.G. (1997). Activation of p53 sequence-specific DNA binding by acetylation of the p53 C-terminal domain. Cell 90, 595–606.

Guidez, F., Howell, L., Isalan, M., Cebrat, M., Alani, R.M., Ivins, S., Hormaeche, I., McConnell, M.J., Pierce, S., Cole, P.A., et al. (2005). Histone acetyltransferase activity of p300 is required for transcriptional repression by the promyelocytic leukemia zinc finger protein. Mol. Cell. Biol. 25, 5552–5566.

Haberland, M., Montgomery, R.L., and Olson, E.N. (2009). The many roles of histone deacetylases in development and physiology: implications for disease and therapy. Nat. Rev. Genet. 10, 32–42.

Halgren, T.A., and Nachbar, R.B. (1996). Merck molecular force field. IV. Conformational energies and geometries for MMFF94. J. Comput. Chem. 17, 587–615.

Hodawadekar, S.C., and Marmorstein, R. (2007). Chemistry of acetyl transfer by histone modifying enzymes: structure, mechanism and implications for effector design. Oncogene 26, 5528–5540.

Hodgkiss, R.J., Begg, A.C., Middleton, R.W., Parrick, J., Stratford, M.R., Wardman, P., and Wilson, G.D. (1991). Fluorescent markers for hypoxic cells. A study of novel heterocyclic compounds that undergo bio-reductive binding. Biochem. Pharmacol. 41, 533–541.

Holbert, M.A., Sikorski, T., Carten, J., Snowflack, D., Hodawadekar, S., and Marmorstein, R. (2007). The human monocytic leukemia zinc finger histone acetyltransferase domain contains DNA-binding activity implicated in chromatin targeting. J. Biol. Chem. 282, 36603–36613.

Hosoya, T., Aoyama, H., Ikemoto, T., Kihara, Y., Hiramatsu, T., Endoc, M., and Suzuki, M. (2003). Dantrolene analogues revisited: General synthesis and specific functions capable of discriminating two kinds of Ca2+ release from sarcoplasmic reticulum of mouse skeletal muscle. Bioorg. Med. Chem. 11, 663–673.

Itoh, Y., Suzuki, T., and Miyata, N. (2008). Isoform-selective histone deacetylase inhibitors. Curr. Pharm. Des. 14, 529–544.

Iyer, N.G., Xian, J., Chin, S.F., Bannister, A.J., Daigo, Y., Aparicio, S., Kouzarides, T., and Caldas, C. (2007). p300 is required for orderly G1/S transition in human cancer cells. Oncogene 26, 21–29.

Kim, J.B., and Lee, Y.-S. (1991). Peptide synthesis with polymer bound active ester. II Synthesis of pyrazolone resin and its applications in acylation reaction. Bull. Korean Chem. Soc. 12, 376–379.

Kim, Y., Tanner, K.G., and Denu, J.M. (2000). A continuous, nonradioactive assay for histone acetyltransferases. Anal. Biochem. 280, 308–314.

Kitz, R., and Wilson, I.B. (1962). Esters of methanesulfonic acid as irreversible inhibitors of acetylcholinesterase. J. Biol. Chem. 237, 3245–3249.

Langner, M., Remy, P., and Bolm, C. (2005). Highly modular synthesis of C1-symmetric aminosulfoximines and their use as ligands in copper-catalyzed asymmetric Mukaiyama-Aldol reactions. Chem. Eur. J. 11, 6254–6265.

Lau, O.D., Courtney, A.D., Vassilev, A., Marzilli, L.A., Cotter, R.J., Nakatani, Y., and Cole, P.A. (2000a). p300/CBP-associated factor histone acetyltransferase processing of a peptide substrate. Kinetic analysis of the catalytic mechanism. J. Biol. Chem. 275, 1953–1959.

Lau, O.D., Kundu, T.K., Soccio, R.E., Ait-Si-Ali, S., Khalil, E.M., Vassilev, A., Wolffe, A.P., Nakatani, Y., Roeder, R.G., and Cole, P.A. (2000b). HATs off: selective synthetic inhibitors of the histone acetyltransferases p300 and PCAF. Mol. Cell 5, 589–595.

Liu, X., Wang, L., Zhao, K., Thompson, P.R., Hwang, Y., Marmorstein, R., and Cole, P.A. (2008a). The structural basis of protein acetylation by the p300/CBP transcriptional coactivator. Nature 451, 846–850.

Liu, Y., Dentin, R., Chen, D., Hedrick, S., Ravnskjaer, K., Schenk, S., Milne, J., Meyers, D.J., Cole, P., Yates, J., 3rd, et al. (2008b). A fasting inducible switch

modulates gluconeogenesis via activator/coactivator exchange. Nature 456, 269–273.

Macek, B., Mann, M., and Olsen, J.V. (2009). Global and site-specific quantitative phosphoproteomics: principles and applications. Annu. Rev. Pharmacol. Toxicol. 49, 199–221.

Mallya, M., Phillips, R.L., Saldanha, S.A., Gooptu, B., Brown, S.C., Termine, D.J., Shirvani, A.M., Wu, Y., Sifers, R.N., Abagyan, R., and Lomas, D.A. (2007). Small molecules block the polymerization of Z alpha1-antitrypsin and increase the clearance of intracellular aggregates. J. Med. Chem. 50, 5357–5363.

Mantelingu, K., Reddy, B.A., Swaminathan, V., Kishore, A.H., Siddappa, N.B., Kumar, G.V., Nagashankar, G., Natesh, N., Roy, S., Sadhale, P.P., et al. (2007). Specific inhibition of p300-HAT alters global gene expression and represses HIV replication. Chem. Biol. 14, 645–657.

Moreau, F., Desroy, N., Genevard, J.M., Vongsouthi, V., Gerusz, V., Le Fralliec, G., Oliveira, C., Floquet, S., Denis, A., Escaich, S., et al. (2008). Discovery of new Gram-negative antivirulence drugs: structure and properties of novel E. coli WaaC inhibitors. Bioorg. Med. Chem. Lett. 18, 4022–4026.

Nemethy, G., Gibson, K.D., Palmer, K.A., Yoon, C.N., Paterlini, G., Zagari, A., Rumsey, S., and Scheraga, H.A. (1992). Energy parameters in polypeptides. 10. Improved geometrical parameters and nonbonded interactions for use in the ECEPP/3 algorithm, with application to proline-containing peptides. J. Phys. Chem. 96, 6472–6484.

Ogryzko, V.V., Schiltz, R.L., Russanova, V., Howard, B.H., and Nakatani, Y. (1996). The transcriptional coactivators p300 and CBP are histone acetyltransferases. Cell 87, 953–959.

Poux, A.N., Cebrat, M., Kim, C.M., Cole, P.A., and Marmorstein, R. (2002). Structure of the GCN5 histone acetyltransferase bound to a bisubstrate inhibitor. Proc. Natl. Acad. Sci. USA 99, 14065–14070.

Qiao, Y., Molina, H., Pandey, A., Zhang, J., and Cole, P.A. (2006). Chemical rescue of a mutant enzyme in living cells. Science 311, 1293–1297.

Ravindra, K.C., Selvi, B.R., Arif, M., Reddy, B.A., Thanuja, G.R., Agrawal, S., Pradhan, S.K., Nagashayana, N., Dasgupta, D., and Kundu, T.K. (2009). Inhibition of lysine acetyltransferase KAT3B/p300 activity by a naturally occurring hydroxynaphthoquinone, plumbagin. J. Biol. Chem. 284, 24453–24464.

Robinson, J.P., editor. (2009). Current Protocols in Cytometry (New York: Wiley Interscience), Online ISSN 1934-9300.

Shechter, D., Dormann, H.L., Allis, C.D., and Hake, S.B. (2007). Extraction, purification and analysis of histones. Nat. Protoc. 2, 1445–1457.

Shia, W.J., Osada, S., Florens, L., Swanson, S.K., Washburn, M.P., and Workman, J.L. (2005). Characterization of the yeast trimeric-SAS acetyltransferase complex. J. Biol. Chem. 280, 11987–11994.

Shogren-Knaak, M.A., Alaimo, P.J., and Shokat, K.M. (2001). Recent advances in chemical approaches to the study of biological systems. Annu. Rev. Cell Dev. Biol. 17, 405–433.

Stimson, L., Rowlands, M.G., Newbatt, Y.M., Smith, N.F., Raynaud, F.I., Rogers, P., Bavetsias, V., Gorsuch, S., Jarman, M., Bannister, A., et al. (2005). Isothiazolones as inhibitors of PCAF and p300 histone acetyltransferase activity. Mol. Cancer Ther. 4, 1521–1532.

Sutton, A., Shia, W.J., Band, D., Kaufman, P.D., Osada, S., Workman, J.L., and Sternglanz, R. (2003). Sas4 and Sas5 are required for the histone acetyltransferase activity of Sas2 in the SAS complex. J. Biol. Chem. 278, 16887–16892.

Szewczuk, L.M., Saldanha, S.A., Ganguly, S., Bowers, E.M., Javoroncov, M., Karanam, B., Culhane, J.C., Holbert, M.A., Klein, D.C., Abagyan, R., and Cole, P.A. (2007). De novo discovery of serotonin N-acetyltransferase inhibitors. J. Med. Chem. 50, 5330–5338.

Tang, Y., Holbert, M.A., Wurtele, H., Meeth, K., Rocha, W., Gharib, M., Jiang, E., Thibault, P., Verreault, A., Cole, P.A., and Marmorstein, R. (2008). Fungal Rtt109 histone acetyltransferase is an unexpected structural homolog of metazoan p300/CBP. Nat. Struct. Mol. Biol. 15, 738–745.

Thomson, S., Clayton, A.L., Hazzalin, C.A., Rose, S., Barratt, M.J., and Mahadevan, L.C. (1999). The nucleosomal response associated with immediate-early gene induction is mediated via alternative MAP kinase cascades: MSK1 as a potential histone H3/HMG-14 kinase. EMBO J. 18, 4779–4793.

Thompson, P.R., Kurooka, H., Nakatani, Y., and Cole, P.A. (2001). Transcriptional coactivator protein p300. Kinetic characterization of its histone acetyltransferase activity. J. Biol. Chem. 276, 33721–33729.

Thompson, P.R., Wang, D., Wang, L., Fulco, M., Pediconi, N., Zhang, D., An, W., Ge, Q., Roeder, R.G., Wong, J., et al. (2004). Regulation of the p300 HAT domain via a novel activation loop. Nat. Struct. Mol. Biol. 11, 308–315.

Totrov, M., and Abagyan, R. (1997). Flexible protein–ligand docking by global energy optimization in internal coordinates. Proteins 1 (Suppl.), 215–220.

Totrov, M., and Abagyan, R. (1999). Derivation of sensitive discrimination potential for virtual ligand screening. Proceedings of the Third Annual International Conference on Computational Molecular Biology, 312–320.

Vasyunkina, T.N., Bykova, L.M., Plotkin, V.N., and Ramsh, S.M. (2005). Synthesis of 1,4-dihydropyrano[2,3-c]pyrazole derivatives. Russ. J. Org. Chem. 41, 742–744.

Walsh, C.T. (2006). Post-translational Modification of Proteins (Greenwood Village, CO: Roberts and Co.).

Wang, L., Tang, Y., Cole, P.A., and Marmorstein, R. (2008). Structure and chemistry of the p300/CBP and Rtt109 histone acetyltransferases: implications for histone acetyltransferase evolution and function. Curr. Opin. Struct. Biol. 18, 741–747.

Yang, X.J., and Seto, E. (2008). Lysine acetylation: codified crosstalk with other posttranslational modifications. Mol. Cell 31, 449–461.

Yoshida, M., Kijima, M., Akita, M., and Beppu, T. (1990). Potent and specific inhibition of mammalian histone deacetylase both in vivo and in vitro by trichostatin A. J. Biol. Chem. 265, 17174–17179.

Yu, M., Magalhães, M.L., Cook, P.F., and Blanchard, J.S. (2006). Bisubstrate inhibition: Theory and application to N-acetyltransferases. Biochemistry 45, 14788–14794.

Zheng, Y., Balasubramanyam, K., Cebrat, M., Buck, D., Guidez, F., Zelent, A., Alani, R.M., and Cole, P.A. (2005). Synthesis and evaluation of a potent and selective cell-permeable p300 histone acetyltransferase inhibitor. J. Am. Chem. Soc. 127, 17182–17183.